Available online at www.sciencedirect.com
ScienceDirect
Trans. Nonferrous Met. Soc. China 25(2015) 1410−1418
Transactions of Nonferrous Metals Society of China
www.tnmsc.cn

Characterization and evaluation of interface in SiC_p/2024 Al composite

Pei LIU[1], Ai-qin WANG[1], Jing-pei XIE[1], Shi-ming HAO[2]

1. School of Materials Science and Engineering, Henan University of Science and Technology, Luoyang 471023, China;
2. School of Physical and Engineering, Zhengzhou University, Zhengzhou 450052, China

Received 25 May 2014; accepted 13 July 2014

Abstract: 35% SiC_p/2024 Al (volume fraction) composite was prepared by powder metallurgy method. The microstructures of SiC_p/Al interfaces and precipitate phase/Al interfaces were characterized by HRTEM, and the interface conditions were evaluated by tensile modules of elasticity and Brinell hardness measurement. The results show that the overall SiC_p/Al interface condition in this experiment is good and three kinds of SiC_p/Al interfaces are present in the composites, which include vast majority of clean planer interfaces, few slight reaction interfaces and tiny amorphous interfaces. The combination mechanism of SiC and Al in the clean planer interface is the formation of a semi-coherent interface by closely matching of atoms and there are no fixed or preferential crystallographic orientation relationships between SiC and Al. $MgAl_2O_4$ spinel particles act as an intermediate to form semi-coherent interface with SiC and Al respectively at the slight reaction interfaces. When the composite is aged at 190 °C for 9 h after being solution-treated at 510 °C for 2 h, numerous discoid-shaped and needle-shaped nanosized precipitates dispersively exist in the composite and are semi-coherent of low mismatch with Al matrix. The Brinell hardness of composites arrives peak value at this time.
Key words: SiC_p/2024 Al composite; interface; precipitate phase; characterization

1 Introduction

Because of their high specific strength and elastic modulus, good wear resistance and low CTE values, metal matrix composites (MMCs) have received much attention in recent years and become attractive as candidate materials in aerospace applications [1,2]. The aluminum matrix composites containing particulate and whiskers of silicon carbide are the most promising materials [3,4]. The load would be transferred from the matrix to the reinforcements by the interface during the deformation process, and thus a strengthening matrix and good bonding interface between reinforcement and matrix are favorable to the mechanical properties.

As the load transfers from the matrix to the reinforcements during the deformation process, the interfacial structures between SiC and Al are critical to control mechanical properties of the composite. It is accepted that good bonding interfaces with coherency or semicoherency are favorable to the mechanical properties, whereas interfaces with incoherency, especially those with the presence of brittle intermetallic phases at the interfaces, degrade these properties [5,6]. During the fabrication of the SiC_p/Al composite, a major technical problem occurs with the formation of Al_4C_3 phase at the interface. This brittle reactant Al_4C_3, in the shape of thin hexagonal platelet, degrades the strength, modulus, and corrosion resistance of the composite. So far, the following methods have been proposed in order to prevent the formation of Al_4C_3 reactant at the SiC_p/Al interface.

1) Addition of excessive Si into the matrix composition. The Si element in the Al melt can effectively inhibit the formation of Al_4C_3 through increasing activity $a_{[Si]}$ of the solution, as evidenced from the following reaction:

$$3SiC(s)+4[Al]=Al_4C_3(s)+3[Si] \quad (1)$$

where the elements in the brackets are in the molten solution. This method is effective but the matrix composition is modified, which may affect the composite global properties [7].

2) Pre-oxidation of SiC to introduce a thin coating layer of SiO_2 on the SiC surface, which is believed to act as an intermediate to form stable interfacial structures

Foundation item: Project (51371077) supported by the National Natural Science Foundation of China
Corresponding author: Ai-qin WANG; Tel: +86-13938881511; E-mail: aiqin_wang888@163.com
DOI: 10.1016/S1003-6326(15)63740-2

that prevent direct contact of SiC and Al. In the presence of SiO_2 layers on the SiC surface, the following reactions may occur in the Al melt containing Mg element:

$$SiO_2(s)+2[Mg]=2MgO(s)+[Si] \quad (2)$$

$$2SiO_2(s)+2[Al]+[Mg]=MgAl_2O_4+2[Si] \quad (3)$$

LIU et al [8] prepared the oxidized SiC_p/Al−Mg alloy composites by squeeze casting. $MgAl_2O_4$ forms on the surface and the interface action can be controlled via SiC_p oxidation technical parameters.

3) Powder metallurgy method. According to the reactivity between SiC particles and molten Al, powder metallurgy becomes an effective way to produce SiC_p/Al composites in solid state by eliminating the reaction between reinforcement and matrix. CHENG et al [9] used a powder metallurgy route followed by hot extrusion to fabricate the SiC_p/Al composites. They found that the reinforcement SiC particles were bonded well with Al matrix through an amorphous layer with thickness of 20−30 nm by diffusion of Al and Mg into SiO_2 layer on the SiC particles. FAN [10] gained the SiC_p/1100 Al and SiC_p/7075 Al composites by powder metallurgy. The results indicated that clean planar interfaces with zero thickness and without morphology change of SiC particles were found in the composites hot-pressed below the solidus temperature of the matrix. Several kinds of interfaces were present in the composites hot-pressed between the melting point and the solidus temperature of the matrix.

For some aluminum alloy matrix composites, especially 2xxx and 6xxx aluminum alloy matrix composites, heat treatment is an effective method to strengthen the matrix because numerous nanosized precipitates can distribute diffusely in the matrix after heat treatment, coherent or semi-coherent with matrix, which can inhibit the dislocation motion and significantly increase properties of some aluminum alloy matrix composites [11−13]. According to Ref. [14], the main strengthening phases of 2024 Al are $\theta(Al_2Cu)$ and $S(Al_2CuMg)$. The addition of reinforcement in aluminum matrix composite does not fundamentally change its aging precipitation process.

From the above analysis, the interface types of SiC_p/Al composites are especially complex, mainly including SiC_p/Al interfaces and different kinds of precipitate/Al interfaces. So, it is important to characterize the interface microstructure in the aluminum matrix composites. In this study, a 35% SiC_p/2024 Al composite (volume fraction) was produced by using the PM technique. The aim of this work is to characterize and evaluate various kinds of interfaces in the composites by transmission electron microscopy (TEM), stress−strain curve and Brinell hardness measurement.

2 Experimental

2.1 Experimental materials

SiC particles (mean particle size of 15 μm) and gas atomized 2024 aluminum powders with an average particle size of 10 μm were used as reinforcement and base alloy, respectively. The chemical composition of 2024 aluminum is listed in Table 1.

Table 1 Chemical composition of 2024 aluminum matrix alloy (mass fraction, %)

Cu	Mg	Mn	Fe	Al
4.4	1.5	0.5	0.1	Bal.

2.2 Experimental process

In this research, the aluminum matrix composite was manufactured by powder metallurgy technique. The powders (35% SiC particles, volume fraction) and balls with the ratio of 2:1 were blended in the Y style mixer for 24 h at the revolving speed of 50 r/min and then the mixed powers were put into the mold and hot-pressed up to 580 °C at 8 °C/min in the VDBF−250 experiment machine with the vacuum degree of 2.3×10^{-3} Pa. The stress of 80 MPa was applied to the powders at 580 °C for 3 h and then the powders were cooled in the furnace with the protection of vacuum. When the temperature dropped to room temperature, the stress was removed and the composite was acquired. The tensile tests of composites were conducted using the Shimadzu AG−I250KN precision universal testing machine at a constant crosshead speed of 1 mm/min.

Various specimens were obtained from the composite and solution-treated at 510 °C for 2 h, water-quenched, and then aged at 190 °C for periods up to 40 h. The age-hardening responses of composite were characterized using Brinell hardness (HB) measurement, with triplicate specimens and five measurements per condition to ensure the accuracy of results. The metallographic samples were ground and polished following standard metallographic practices, and then were etched using Keller's reagent (1 mL HF+1.5 mL HCl+2.5 mL HNO_3+95 mL H_2O). The samples for TEM observation were machined into 0.5 mm by wire-electrode cutting and ground to 50 μm by mechanical thinning, and then cut into foils with 3 mm in diameter. After that, foils were prepared by argon ion milling using Gatan 691 precision ion polishing system. Transmission electron microscopy (TEM) investigations were performed on a JEM−2100 HRTEM microscope operated at 200 kV.

3 Results and discussion

3.1 Structure of SiC

Figure 1(a) shows the SEM image of the SiC

powders used in the present study. The SiC particles are angular. Diffraction patterns and high resolution TEM images show that both hexagonal α-SiC and cubic β-SiC are present in the composites. The hexagonal allotrope has predominantly the $6H_\alpha$ poly type structure. Figures 1(b) and (c) show a high resolution TEM image and the corresponding SAED pattern of the 6H α-SiC along $[2\bar{1}\bar{1}0]$ zone axis. In Fig. 1(b), the interplanar spacing of (001) plane in 6H α-SiC phase is 1.51 nm. Each (001) plane consists of six layers and the stacking sequence is *ABCACB*. Then, the interplanar spacing of each atomic layer is 0.251 nm. Figures 1(d) and (e) show a high resolution TEM image and the corresponding SAED pattern of the cubic β-SiC along [001] zone axis.

3.2 Interface between SiC and Al

3.2.1 Clean interface between SiC and Al

Figures 2(a) and (b) show the typical interface morphologies of SiC_p/2024 Al alloy matrix in this experiment. We can see from Figs. 2(a) and (b) that the interfaces are clean and smooth, and there are no interface reactants and the phenomenon of SiC particles dissolved. Previous studies [15,16] have shown that SiC particles are easy to react with Al to generate Al_4C_3 in the SiC particles reinforced aluminum alloy matrix composites. But we did not find Al_4C_3 reactants in the composite materials in this experiment, because the hot-press sintering technology was used, the temperature throughout was too low to produce interface chemical

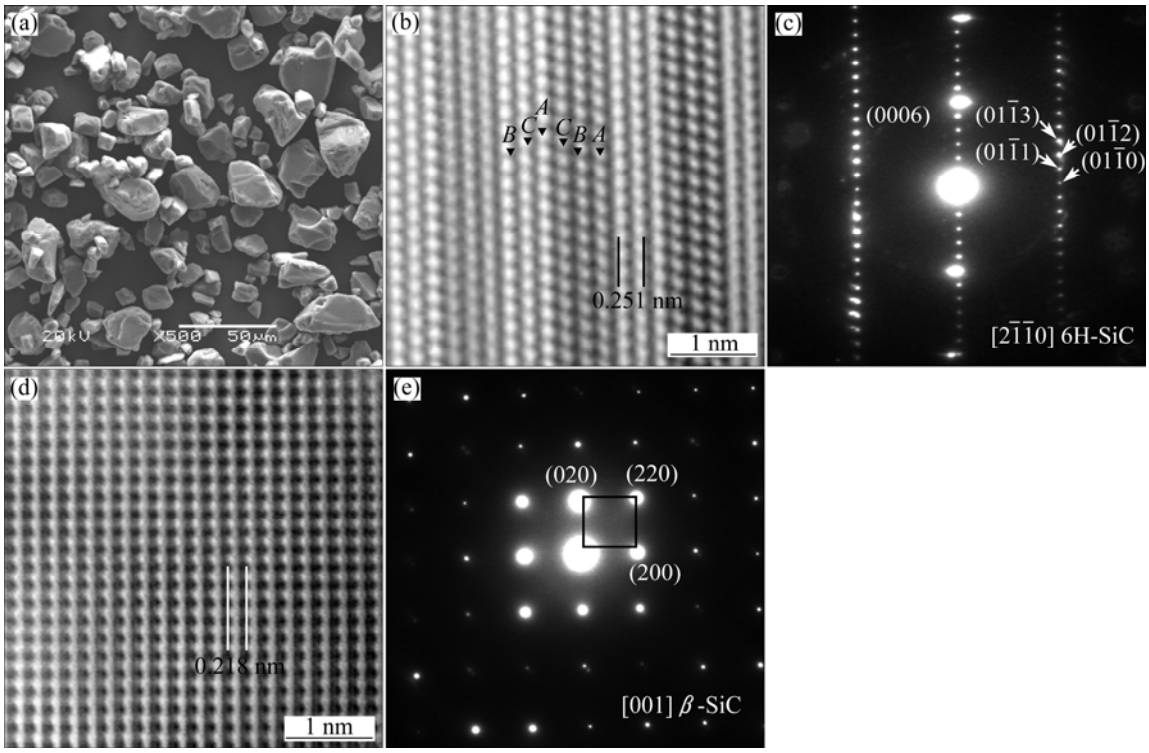

Fig. 1 SEM image of SiC powder and HRTEM images of SiC in composite: (a) SEM image of SiC powder; (b) HRTEM image of 6H α-SiC; (c) Corresponding SAED pattern of 6H α-SiC; (d) HRTEM image of β-SiC; (e) Corresponding SAED pattern of β-SiC

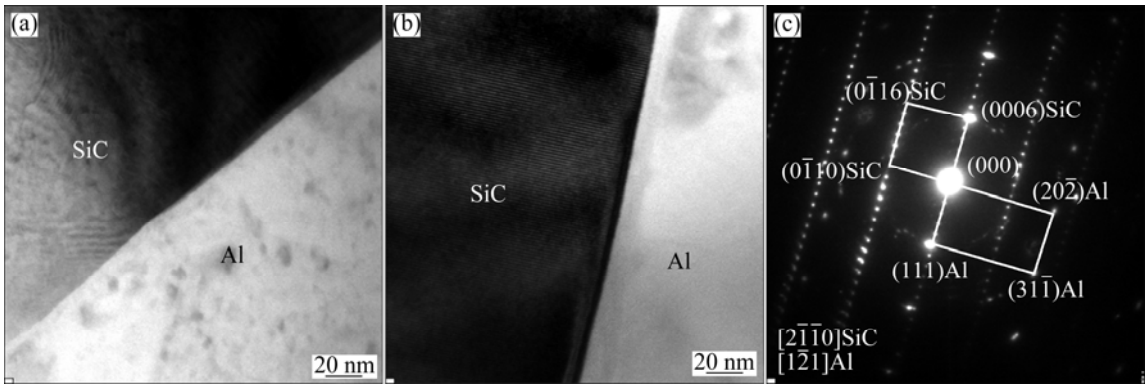

Fig. 2 TEM image and SAED pattern of clean interface between SiC and Al: (a) TEM image of clean interface observed in one area; (b) TEM image of clean interface observed in another area; (c) SAED pattern of 6H α-SiC and Al

reaction. So, the interface of the composite is clean, which provides the prerequisites for the composite material with excellent performance.

Figure 2(c) shows a selected area electron diffraction (SAED) pattern from the Al phase along $[1\bar{2}1]$ zone axis and the 6H SiC phase along $[2\bar{1}\bar{1}0]$ zone axis. As calibrated in Fig. 2(c), the close-packed (111) plane of the Al phase is parallel to the close-packed basal plane (0001) of the SiC phase, and thus their OR, denoted as OR I in this work, is determined as follows: $[2\bar{1}\bar{1}0]$ SiC//$[1\bar{2}1]$ Al, (0001) SiC//(111) Al. The interplanar spacing of (111) planes in the Al phase is 0.234 nm, while the interplanar spacing of (0006) planes in α-SiC phase is 0.251 nm, and the lattice misfit between them is 0.07. It is obvious that the combination mechanism of SiC and Al is the formation of a semi-coherent interface by closely matching of atoms.

Figure 3(a) gives a HRTEM image of the interface between the reinforcement particle and the matrix. The interface, as indicated in Fig. 3(a), is very clean, smooth and straight. No reaction product has been found at the interface. The IFFT images of 6H α-SiC phase along $[2\bar{1}\bar{1}0]$ zone axis and Al along [001] zone axis are respectively shown in Figs. 3(b) and (c). Figures 3(d) and (e) are corresponding SAED and its indexed patterns, respectively. In Fig. 3(e), the circles represent the reflections from the matrix and the dots represent those from SiC particles. The incident beam is parallel to [001] Al and $[2\bar{1}\bar{1}0]$ 6H α-SiC, and the (020) plane of the matrix Al is parallel to the plane $(01\bar{1}3)$ of the SiC phase. Thus, their OR, denoted as OR II in this work, is determined as follows: $[2\bar{1}\bar{1}0]$ SiC//[001] Al, $(0\bar{1}13)$ SiC//(020) Al. The interplanar spacing of (020) planes in the matrix is 0.203 nm, while the interplanar spacing of $(01\bar{1}3)$ planes in α-SiC phase is 0.235 nm. Figure 3(f) shows the IFFT image of square area in Fig. 3(a), which gives a semi-coherent interface where every seven (200) Al atoms corresponding to six $(01\bar{1}3)$ α-SiC atoms with a mismatch of less than 1%.

A second high resolution image of the interface between the reinforcement particle and the matrix is also observed, as shown in Fig. 4(a). In the SAED pattern in Fig. 4(b), the SiC is along $[45\bar{1}3]$ zone axis and Al along [001] zone axis. The (020) plane of the matrix Al is parallel to the plane $(\bar{1}103)$ of the SiC phase, as indexed in Fig. 4(c). Thus, the following OR III results are $[45\bar{1}3]$ SiC//[001] Al, $(\bar{1}103)$ SiC//(020) Al.

Figure 4(f) shows the IFFT image of square area in Fig. 4(a), the interplanar spacing of (020) planes in the matrix is 0.202 nm, while the interplanar spacing of $(\bar{1}103)$ planes in 6H α-SiC phase is 0.255 nm, which also gives a semi-coherent interface between 6H α-SiC and Al matrix.

3.2.2 Slight reaction interface between SiC and Al

A type of slight reaction interface is also observed, although less frequently, as shown in Fig. 5(a). A

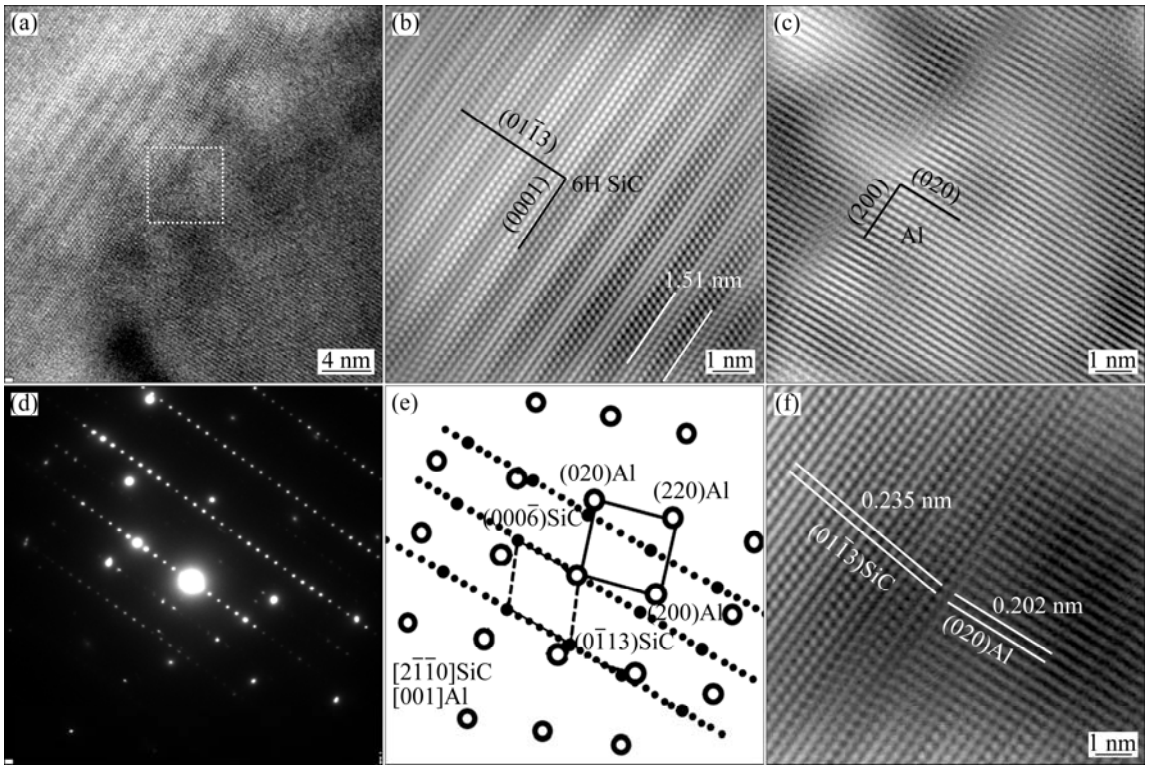

Fig. 3 HRTEM image of clean interface between SiC and Al showing OR II between them: (a) Initial HRTEM image of interface between SiC and Al; (b) IFFT image of 6H α-SiC; (c) IFFT image of Al; (d) Corresponding SAED pattern of interface; (e) Indexed patterns; (f) IFFT image of square area in Fig. 3(a)

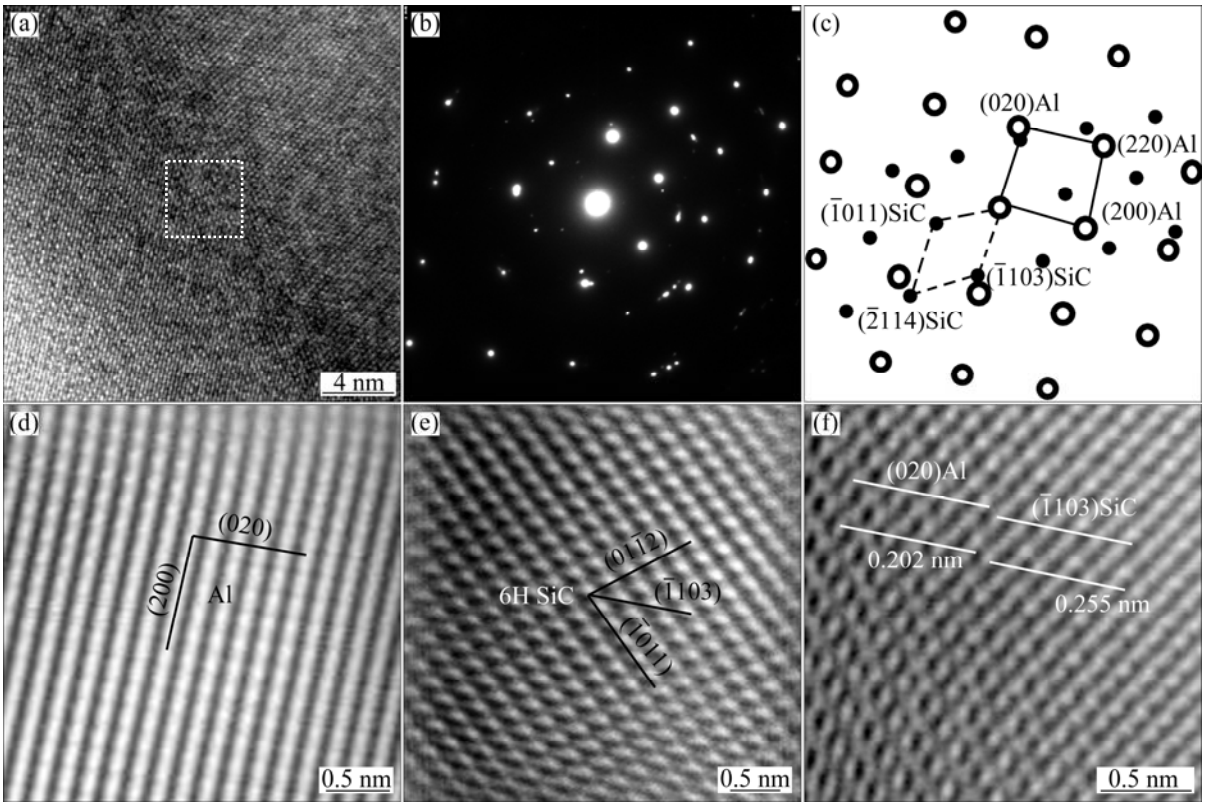

Fig. 4 HRTEM image of clean interface between SiC and Al showing OR III between them: (a) Initial HRTEM image of interface between SiC and Al; (b) Corresponding SAED pattern of interface; (c) Indexed patterns; (d) IFFT image of Al; (e) IFFT image of 6H α-SiC; (f) IFFT image of square area in Fig. 4(a)

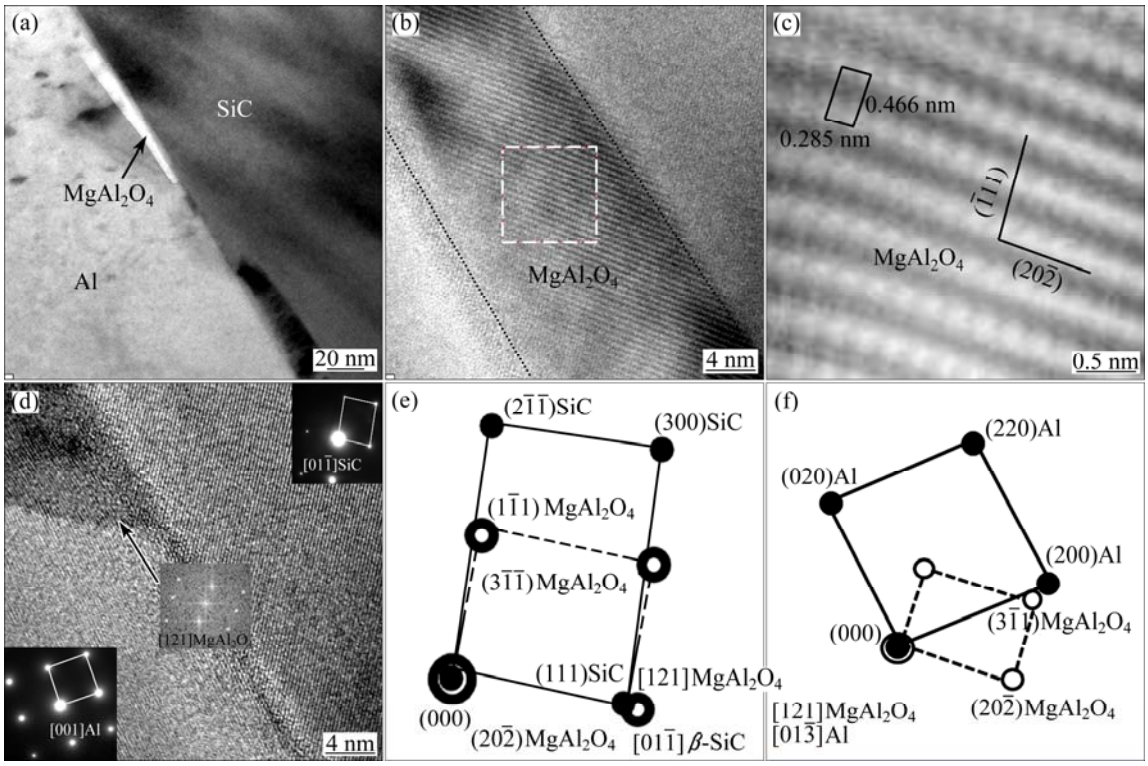

Fig. 5 Slight reaction interface between SiC and Al: (a) TEM image of slight reaction interface; (b) HREM image of $MgAl_2O_4$; (c) IFFT image of square area in Fig. 5(b); (d) HRTEM image of SiC/$MgAl_2O_4$/Al interface; (e) Indexed patterns of $MgAl_2O_4$ and β-SiC; (f) Indexed patterns of $MgAl_2O_4$ and Al

nanocrystalline particle with the length of about 100 nm and width of about 10 nm was found at the interface between SiC and Al. Figure 5(b) shows the HRTEM image of nanocrystalline particle, and Fig. 5(c) shows the IFFT image of square area in Fig. 5(b). The arrangement of the atomic structure of the nanocrystalline particle can clearly be observed from the IFFT image (Fig. 5(c)). As shown in Fig. 5(c), the smallest quadrilateral element was selected. After being accurately measured, the length and width were respectively indexed to be consistent with the interplanar spacing of $(20\bar{2})$ planes and $(1\bar{1}1)$ planes in $MgAl_2O_4$, thus the nanocrystalline particle is identified as $MgAl_2O_4$ (space group $Fd3m$, lattice parameter a=0.81 nm). The $MgAl_2O_4$ phase has been extensively reported in the literature in a rather wide variety of studies, and there existed a SiO_2 membrane with a thickness of about 5 nm on the surface of commercial SiC particles. In the presence of SiO_2 layers on the SiC surface, the following reactions may occur in the Al matrix containing Mg element:

$$3SiO_2+4Al=2Al_2O_3+3Si \quad (4)$$

$$SiO_2+2Mg=2MgO+2Si \quad (5)$$

$$Al_2O_3+MgO=MgAl_2O_4 \quad (6)$$

The sintering temperature in this study was 580 °C and slightly higher than the solidus temperature of 2024 Al. So, few of 2024 Al powders would melt and then the above three response equations would occur in the process of vacuum hot-pressing.

Figure 5(d) shows the HRTEM image of $SiC/MgAl_2O_4/Al$ interfaces, Figs. 5(e) and (f) are respectively the corresponding indexed patterns of $SiC/MgAl_2O_4$ and $MgAl_2O_4/Al$. It can be seen from Fig. 5(e) that the lattice plane $(20\bar{2})$ of $MgAl_2O_4$ is parallel to lattice plane (111) of β-SiC. The interplanar spacing of $MgAl_2O_4$ on lattice plane $(20\bar{2})$ is 0.285 nm and that of β-SiC on lattice plane (111) is 0.252 nm. The lattice misfit between them is 0.116, which indicates the semi-coherent interface between β-SiC and $MgAl_2O_4$.

Figure 5(f) indicates that the lattice plane $(3\bar{1}\bar{1})$ of $MgAl_2O_4$ is parallel to lattice plane (200) of Al. The interplanar spacing of $MgAl_2O_4$ on lattice plane $(3\bar{1}\bar{1})$ is 0.244 nm and that of Al on lattice plane (200) is 0.202 nm. The lattice misfit between them is 0.17, which indicates the semi-coherent interface between Al matrix and $MgAl_2O_4$. The semi-coherent interface of $SiC/MgAl_2O_4$ and $MgAl_2O_4/Al$ indicates that $MgAl_2O_4$ spinel particles act as an intermediate to form stable interfacial structures.

3.2.3 Amorphous interface between SiC and Al

Figure 6(a) shows the HRTEM image of little amorphous interface between SiC and Al in the composite. It can be clearly observed from Fig. 6(a) that an amorphous interface with about 15 nm in thickness exists between SiC and Al. The IFFT images of three square areas 1, 2 and 3 in Fig. 6(a) are respectively corresponding to 6H α-SiC phase along $[45\bar{1}3]$ zone axis, amorphous diffraction pattern and Al matrix along $[\bar{1}12]$ zone axis. Some studies [9,10] have shown that the production of amorphous layer is connected with the magnesium concentration at the interface and the formation of impurity phase. There exists a SiO_2 membrane with about 5 nm in thickness on the surface of commercial SiC particles, the sintering temperature in this study was 580 °C and slightly higher than the solidus temperature of 2024 Al. So, few of 2024 Al powders would melt, Mg element is easy to enrich at the interface and generate impurity phase and oxide layer during the solidification of liquid matrix.

3.3 Interface between precipitated phase and Al

Figure 7 shows the TEM micrographs of SiC_p/2024 Al composite aged at 190 °C for 9 h after solution-treated at 510 °C for 2 h. It can be seen from Figs. 7(a) and (b) that numerous discoid-shaped nanoscale precipitates with the diameter ranging from 50 to 200 nm, needle-shaped nanoscale precipitates with the average length of 100−150 nm distributed homogeneously and dispersively in the composite.

Figure 8 shows the TEM image of precipitates and the HRTEM images of interface between precipitates and

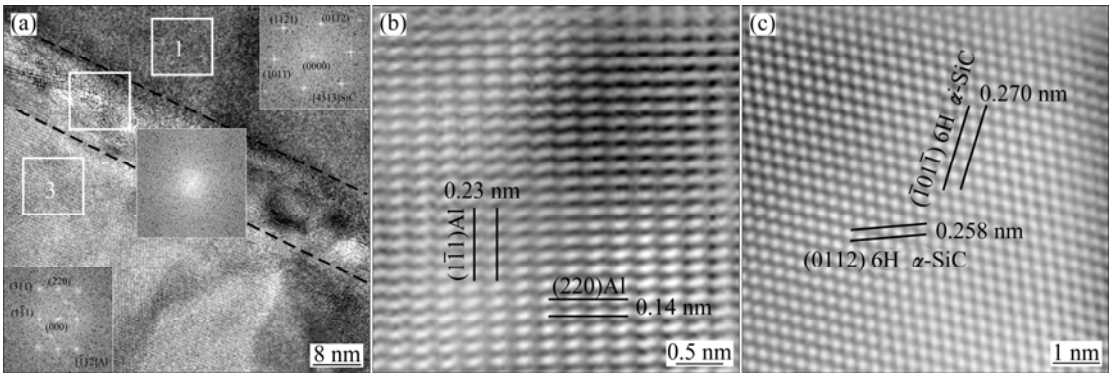

Fig. 6 Amorphous interface between SiC and Al: (a) HRTEM image of amorphous interface; (b) IFFT image of Al; (c) IFFT image of 6H α-SiC

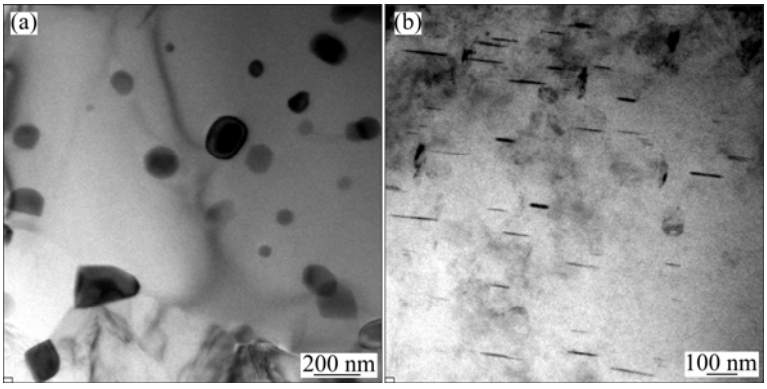

Fig. 7 TEM micrographs of composite aged at 190 °C for 9 h after solution-treated at 510 °C for 2 h: (a) Discoid-shaped nanoscale precipitates; (b) Needle-shaped nanoscale precipitates

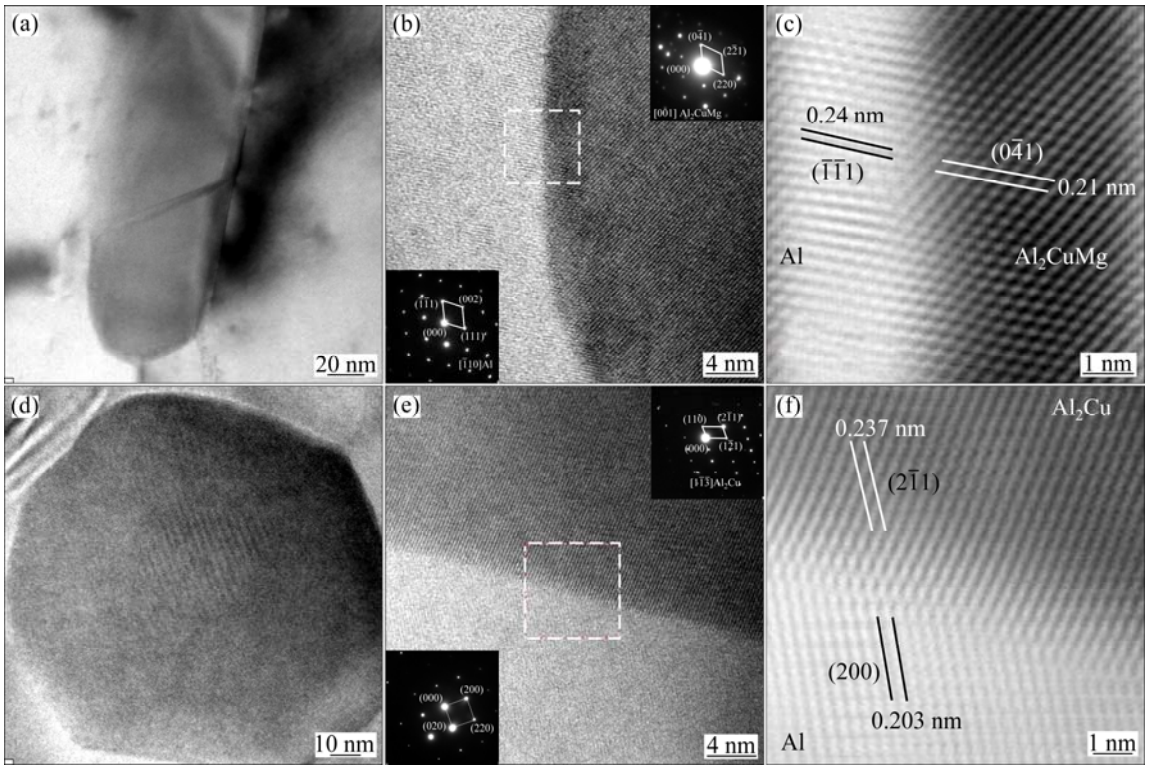

Fig. 8 TEM image of precipitates and HTREM images of interface between precipitates and Al matrix: (a) TEM image of Al_2CuMg; (b) HRTEM image of interface between Al_2CuMg and Al; (c) IFFT image of square area in Fig. 8(b); (d) TEM image of Al_2Cu; (e) HRTEM image of interface between Al_2Cu and Al; (f) IFFT image of square area in Fig. 8(e)

Al matrix. The diffraction patterns from needle-shaped nanoscale particles (see Fig. 8(b)) were indexed to be consistent with Al_2CuMg (Space group: *Cmcm*; lattice parameters: a=4.008 Å, b=9.248 Å, c=7.154 Å) and diffraction pattern from discoid-shaped nanoscale particles (see Fig. 8(e)) was indexed to be consistent with Al_2Cu (Space group: $p\bar{4}3m$; lattice parameters: a=8.704 Å). Figures 8(c) and (f) respectively show the IFFT images of square areas in Figs. 8(b) and (e). It can be clearly observed from the IFFT images that the lattice plane $(\bar{1}\,\bar{1}\,1)$ of Al is parallel to lattice plane (0$\bar{4}$1) of Al_2CuMg, and the lattice plane (200) of Al is parallel to lattice plane (2$\bar{1}$1) of Al_2Cu. The interplanar spacing of Al on lattice plane $(\bar{1}\,\bar{1}\,1)$ is 0.24 nm and that of Al_2CuMg on lattice plane (0$\bar{4}$1) is 0.21 nm. The lattice misfit between them is 0.125, which indicates the semi-coherent interface between Al and Al_2CuMg. Similarly, the interplanar spacing of Al on lattice plane (200) is 0.203 nm and that of Al_2Cu on lattice plane $(2\,\bar{1}\,1)$ is 0.237 nm. The lattice misfit between them is 0.143, which also indicates the semi-coherent interface between Al and Al_2Cu.

3.4 Evaluation of interfaces in composite

Some researchers [17] applied a method to evaluate particle–matrix bonding of particulate reinforced aluminum matrix composites by measuring the change in elastic modulus of composite with increasing plastic strain. There are a lot of reports [18,19] about the theoretical prediction model of elastic modulus of particles reinforced metal matrix composites, among them, Hashin−Shtrikman model has been accepted by more and more researchers [20]. The model indicates the elastic modulus of the composite as follows:

$$E_c = E_m \frac{E_m\varphi_m + E_r(\varphi_r + 1)}{E_r\varphi_m + E_m(\varphi_r + 1)} \quad (7)$$

where E_c is the elastic modulus of the composite material; E_m and φ_m are the elastic modulus and volume fraction of matrix, respectively; E_r and φ_r are the elastic modulus and volume fraction of reinforcement, respectively.

Figure 9(a) shows the elastic deformation curves of model results and experiment. It can be seen clearly that the theoretical curve and experimental curve match very well，which indicates good bonding interfaces between SiC and Al in this experiment. Figure 9(b) shows age hardening curve of the composite at different aging time.

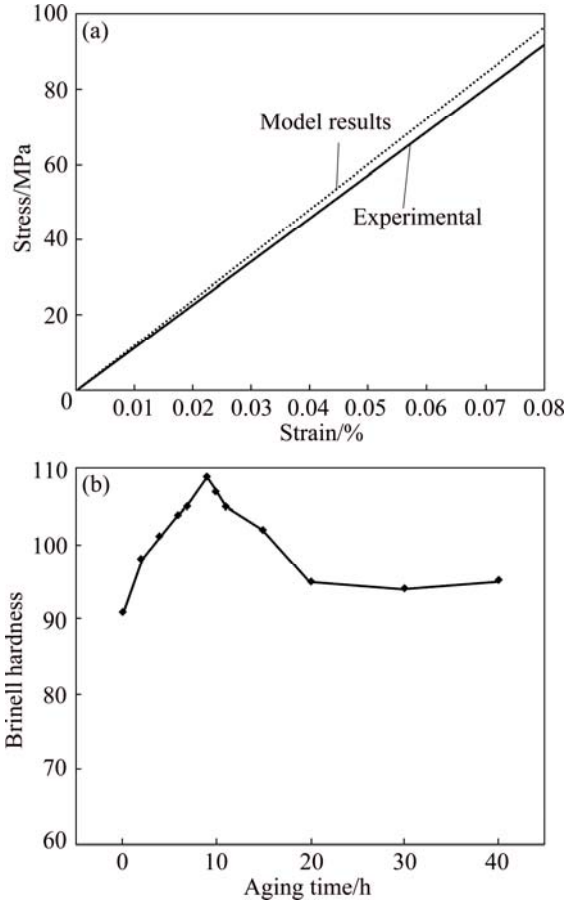

Fig. 9 Comparison of experimental elastic deformation curve of composite with theoretical curve (a) and age hardening curve of composite at different aging time (b)

The Brinell hardness arrived peak when composite was aged for 9 h. As described in Section 3.3, numerous nanosized precipitates distributed diffusely in the matrix after being aged for 9 h and were semi-coherent with matrix. The semi-coherent interface between Al and precipitates can inhibit the dislocation motion and thus gives a great help of the strength improvement.

4 Conclusions

1) The overall interface condition in this experiment is good. Three kinds of SiC/Al interfaces are present in the composites, which include vast majority of clean planer interfaces, few slight reaction interfaces and tiny amorphous interfaces.

2) The combination mechanism of SiC and Al in the clean planer interface is the formation of a half coherent interface by closely matching of atoms. There are no fixed or preferential crystallographic orientation relationships between SiC and Al. $MgAl_2O_4$ spinel particles act as an intermediate to form stable interfacial structures at the slight reaction interfaces.

3) When the composite was aged at 190 °C for 9 h after solution-treatment at 510 °C, numerous discoid-shaped and needle-shaped nanosized precipitates existed in the composite. The Brinell hardness of composites arrived peak at this time.

References

[1] ZHU Xiao-min, YU Jia-kang, WANG Xin-yu. Microstructure and properties of Al/Si/SiC composites for electronic packaging [J]. Transactions of Nonferrous Metals Society of China, 2012, 22(7): 1686−1692.

[2] DURBADAL M, SRINATH V. Effect of heat treatment on microstructure and interface of SiC particle reinforced 2124 Al matrix composite [J]. Materials Characterization, 2013, 85: 73−81.

[3] OMYMA E K, FATHY A. Effect of SiC particle size on the physical and mechanical properties of extruded Al matrix nanocomposites [J]. Materials and Design, 2014, 54: 348−353.

[4] MAZAHERY A, SHABANI M O. Microstructural and abrasive wear properties of SiC reinforced aluminum-based composite produced by compocasting [J]. Transactions of Nonferrous Metals Society of China, 2013, 23(7): 1905−1914.

[5] LUO Z P. Crystallography of SiC/$MgAl_2O_4$/Al interfaces in a pre-oxidized SiC reinforced SiC/Al composite [J]. Acta Materialia, 2006, 54(1): 47−58.

[6] NIE Cun-zhu, GU Jia-jun, LIU Jun-liang, ZHANG Di. Investigation on microstructures and interface character of B_4C particles reinforced 2024 Al matrix composites fabricated by mechanical alloying [J]. Journal of Alloys and Compounds, 2008, 454(1−2): 118−122.

[7] LEE J C, PARK S B, SEOK H K, OH C S, LEE H I. Prediction of Si content to suppress the interfacial reaction in the SiC_p/2014 Al composites [J]. Acta Materialia, 1998, 46(8): 2635−2643.

[8] LIU Jun-you, LIU Ying-cai, LIU Guo-quan, YIN Yan-sheng, SHI Zhong-liang. Oxidation behavior of silicon carbide particles and their interfacial characterization in aluminum matrix composites [J]. The Chinese Journal of Nonferrous Metals, 2002, 12(5): 897−902. (in Chinese)

[9] CHENG Nan-pu, ZENG Su-min, LIU Zhi-yi. preparation, microstructures and deformation behavior of SiC_p/6066 Al composites produced by PM route [J]. Journal of Materials Processing Technology, 2008, 202(1−3): 27−40.
[10] FAN Jian-zhong. Interfacial condition and deformation behavior of PM SiC_p/Al composites [D]. Harbin: Harbin Institute of Technology, 1999: 44−75. (in Chinese)
[11] BEKHEET N, GADELRAB R, SALAH M, ABDEL A. The effects of aging on the hardness and fatigue behavior of 2024 Al alloy/SiC composites [J]. Materials and Design, 2002, 23(2): 153−159.
[12] PAL S, MITRA R, BHANUPRASAD V V. Aging behavior of Al−Cu−Mg alloy−SiC composites [J]. Materials Science and Engineer A, 2008, 480(1−2): 496−505.
[13] MA S M R, SR S M. Aging behavior of a 2024 Al alloy SiC_p composite [J]. Materials and Design, 2010, 31(5): 2368−2374.
[14] TIAN Rong-zhang, WANG Zhu-tang. Aluminum alloy and its processing manual (II) [M]. Changsha: Central South University Press, 2000: 14−16. (in Chinese)
[15] HE Yi-qiang, WANG Na, QIAO Bin, FENG Li-chao, CHEN Zhi-gang, CHEN Zhen-hua. SiC/Al interface feature of Al−Fe−V−Si alloy reinforced with SiC particles [J]. The Chinese Journal of Nonferrous Metals, 2010, 20(7): 1302−1308. (in Chinese)
[16] ZHANG Shao-qin, CUI Yan, SONG Ying-gang. Microstructural study of SiC_p/Al composite prepared by pressureless infiltration [J]. Journal of Materials Engineering, 2000, 10: 3−7. (in Chinese)
[17] KENNEDY A R, WYATT S M. Characterising particle matrix interfacial bonding in particulate Al−TiC MMCs produced by different methods [J]. Composites: Part A, 2001, 32: 555−559.
[18] SUN L Z, JU J W, LIU H T. Elastoplastic modeling of metal matrix composites with evolutionary particle debonding [J]. Mechanics of Materials, 2003, 35(3−6): 559−569.
[19] LU Ping, LIU Zuo-min. Mixed-mode of elastic modulus composites based on the α factor [J]. Journal of Wuhan University of Technology, 2008, 30(9): 19−22. (in Chinese)
[20] BARRIE D. New materials in space [J]. Material World, 2000(1): 13−15.

SiC_p/2024 Al 复合材料界面的表征及评价

柳 培[1]，王爱琴[1]，谢敬佩[1]，郝世明[2]

1. 河南科技大学 材料科学与工程学院，洛阳 471023；
2. 郑州大学 物理工程学院，郑州 450052

摘 要：采用粉末冶金方法制备体积分数为 35%的 SiC_p/2024 Al 复合材料。利用高分辨透射电镜对复合材料中 SiC_p 与 Al 基体、析出相与 Al 基体之间的界面微结构进行表征，采用拉伸弹性模量和布氏硬度测试对界面状况进行评估。结果表明，所得复合材料中 SiC 与 Al 的界面整体状况良好。复合材料中 SiC/Al 界面分为 3 种类型：大部分干净界面、少量轻微反应型界面以及极少量的非晶层界面。在干净界面中，SiC 和 Al 的结合机制为紧密原子匹配形成的半共格界面，且 SiC 和 Al 无固定或择优的取向关系。在轻微反应型界面中，$MgAl_2O_4$ 尖晶石与 SiC 和 Al 均形成半共格界面，作为中间媒介很好地连接 SiC 和 Al。复合材料经 510 ℃ 固溶 2 h 再在 190 ℃ 时效 9 h 后，许多圆盘状纳米析出相和棒针状纳米析出相弥散分布于基体中，且与基体的界面为错配度较小的半共格界面。此时，复合材料的布氏硬度达到峰值。

关键词：SiC_p/2024 Al 复合材料；界面；析出相；表征

(Edited by Wei-ping CHEN)